PERGAMON

International Journal of Multiphase Flow 28 (2002) 911–925

International Journal of Multiphase Flow

www.elsevier.com/locate/ijmulflow

Strong squeezing flow between parallel plates leads to rolling motion at the contact line

S.N. Reznik, A.L. Yarin *

Faculty of Mechanical Engineering, Technion, Israel Institute of Technology, Haifa 32000, Israel

Received 17 December 2000; received in revised form 13 January 2002

Abstract

Squeezing of a droplet between a pair of plates serves as an experimental method for probing the dynamics of moving contact lines (CL). It is also indicative of a possible interplay between inner-scale effects and the bulk flow hydrodynamics. In this paper strong squeezing of a two-dimensional liquid droplet between parallel plates moving against each other is studied in the inertialess approximation. It is shown that the dynamics of the moving CL is mainly governed by the macroscopic bulk flow, whereas molecular slip and wetting in the vicinity of the CL have a minor effect. As a result, the apparent contact angle continuously increases, and after some time rolling motion inevitably sets in. After a longer time, the shape of the free surface tends to become close to circular, albeit distinct from a circle. This is because at the late stage of squeezing, the shape of the free surface is determined mainly by the viscous stresses, which dominate capillary stresses due to the surface tension.

Keywords: Squeezing flow; Droplets; Moving contact line; Apparent contact angle

1. Introduction

Squeezing flow between parallel plates is encountered in many technical applications. Squeezing of a liquid droplet between a pair of plates is one of the simplest experimental methods for the investigation of the motion of contact lines (CL) (Dussan, 1979). Under sufficiently strong squeezing an interplay of two effects is expected in this case, where the hydrodynamic outer-scale bulk flow coexists with the molecular phenomena characteristic of the inner scale near the CL. Existing experimental data do not allow the indentification of any inner-scale mechanism whose nature remains a matter of speculation. According to Somalinga and Bose (2000)

* Corresponding author. Tel.: +972-4-8293-473; fax: +972-4-8324-533.
E-mail address: meralya@yarin.technion.ac.il (A.L. Yarin).

0301-9322/02/$ - see front matter
PII: S0301-9322(02)00014-9

"... measurements made at an outer length scale cannot be used to uniquely delineate inner-scale physics because of inherent difficulties associated with probing inner length scale physics experimentally ...". It is widely accepted that the inner-scale physics is quite complex. Both purely hydrodynamic (Cox, 1986) and molecular-kinetic local effects (Blake, 1993) are responsible for the CL motion, and it is probable that both mechanisms contribute. At sufficiently low bulk velocities the approaches of Cox (1986) and Blake (1993) describe the CL motion accurately (Hayes and Ralston, 1993), whereas at higher velocities their predictions deviate from the empirical Hoffman's law (Hoffman, 1975). The deviation, however, concerns the bulk flow effects.

In Laun et al. (1999), creeping flow in a narrow gap between parallel plates moving against each other was investigated. A partial wall-slip model was applied, and a simple analytical solution was derived based on it. The dependence of the external force needed for squeezing on the squeezing rate and the spacing of the plates, was deduced. The effect of the surface tension acting at the free liquid surface was not accounted for, and CL motion was not considered in detail.

In the present work, the capillary effects at the free liquid surface in the gap are incorporated. The time evolution of the free surface and the CL motion are considered in detail. The squeezing is assumed to be so strong that rolling motion occurs near the moving CL. It is also shown that, at the remote stage of squeezing, the shape of the free surface is determined mainly by the viscous stresses which dominate those related to the surface tension.

The problem of droplet squeezing between two plates is relevant in the context of drop impact/spreading on a horizontal or an inclined plane wall (Yarin and Weiss, 1995; Weiss and Yarin, 1999; Rioboo et al., 2001 and references therein), as well as in the alignment of matched components during the assembly process in optoelectronics and MEMS (Harsh et al., 1999; Patra et al., 1995). It is also relevant to stability of liquid bridges supported by two disks in the situation of interest for material processing in floating zones (Babsky et al., 1987; Bezdenejnykh et al., 1999; Zayas et al., 2000).

In Section 2, the problem of droplet squeezing between two walls is posed. A numerical algorithm is briefly described in Section 3. The results are discussed in Section 4, and conclusions are drawn in Section 5.

2. Formulation of the problem

Consider a two-dimensional droplet of an incompressible viscous liquid placed between parallel plates. The initial shape of the droplet surface is given by two circular arcs with the apparent contact angles between the tangents to the droplet surface and the plates equal to a stationary value α_s. The initial length of the droplet along the plates is $2l_0$ and the initial height is $2h_0$ (Fig. 1). If the plates move against each other with a constant velocity $2V$, the liquid spreads in the horizontal direction. We shall investigate the evolution of the free surface of the droplet. To estimate the characteristic Reynolds number for this problem, we take the liquid density $\rho = 10$ g/cm^3, the viscosity $\mu = 10$ g/cm s, the half-gap $h_0 = 0.1$ cm and the squeeze velocity $V = 1$ cm/s. Then the Reynolds number is

$$Re = \frac{\rho V h_0}{\mu} \sim 0.1. \tag{1}$$

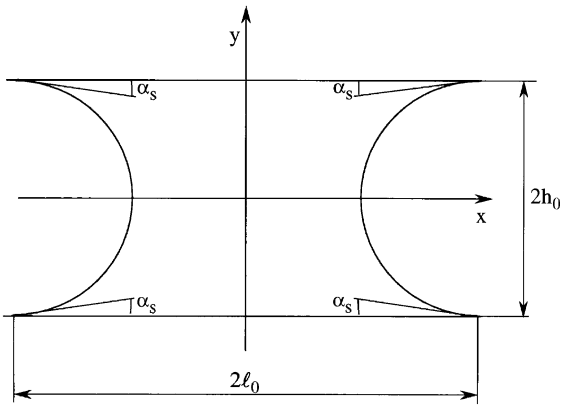

Fig. 1. Scheme of squeezing flow between two parallel plates.

In addition, if we take as the characteristic time scale $T = h_0/V$, then the ratio of the non-stationary term in the Navier–Stokes equation to the viscous one, $\gamma = \rho h_0^2/(\mu T)$, is of the same order as *Re*, which means that $\gamma \sim 0.1$. With the inertial effects neglected, the problem may be considered in the framework of the creeping-flow Stokes equations

$$\nabla p = \mu \Delta \mathbf{u}, \tag{2}$$

$$\nabla \cdot \mathbf{u} = 0, \tag{3}$$

where $\mathbf{u} = (u_x, u_y)$ is the velocity vector, u_x and u_y being the velocity components in the x- and y-directions, and p the pressure, and the gravity effects are neglected. In terms of the stress tensor, the equations of motion (2) and (3) reduce to

$$\frac{\partial \Pi_{ik}}{\partial x_k} = 0, \tag{4}$$

where

$$\Pi_{ik} = -p\delta_{ik} + \mu\left(\frac{\partial u_i}{\partial x_k} + \frac{\partial u_k}{\partial x_i}\right). \tag{5}$$

Squeezing takes place in the time interval $0 \leqslant t < h_0/V$, until the plates come into contact. The model would cease to apply even earlier if the transient Reynolds number $Re_t(t) = \rho V h(t)/\mu$ exceeds 1, but the results discussed in Section 4 show that this is impossible.

We also neglect gravity effects, which assumes that the liquid flow is symmetric about the axes of coordinates. For this reason, we need to consider only the quadrant bounded by the axes $x = 0$ and $y = 0$, as well as by the upper plate and the free surface. The boundary conditions on the upper plate are

$$u_x = 0, \quad u_y = \frac{\mathrm{d}h}{\mathrm{d}t} = -V, \qquad \text{at } y = h(t),\ 0 \leqslant x \leqslant a(t), \tag{6}$$

where V is the absolute velocity of the upper plate relative to the fixed y-axis (cf. Fig. 1), h is the instantaneous half-gap between the plates, and a the horizontal coordinate of the CL. These

conditions do not apply at the CL, in the vicinity of which the continuous approach fails. It is well known that a non-integrable force singularity occurs at the CL if no-slip conditions (6) are assumed (Dussan and Davis, 1974). To avoid this singularity, the Navier–Maxwell slip boundary condition

$$u_x - \lambda \frac{\partial u_x}{\partial y} = 0, \quad y = h(t), \text{ at } x \text{ close to } a(t) \tag{7}$$

can be applied instead of (6). Here λ is a molecular slip coefficient, which is small relative to the characteristic macroscopic length scale of the problem, say h_0. Its dimensionless counterpart $\overline{\lambda} = \lambda/h_0 \ll 1$. The following law of CL motion was deduced (Cox, 1986)

$$\frac{\mu U}{\sigma} = \epsilon\{G(\alpha) - G(\alpha_s)\} + O(\epsilon^2), \tag{8}$$

where

$$G(\alpha) = \int_0^{\alpha} \frac{t - \sin(t)\cos(t)}{2\sin(t)} \mathrm{d}t, \tag{9}$$

$$\epsilon = -\frac{1}{\ln \overline{\lambda}} \ll 1. \tag{10}$$

Here $U = \mathrm{d}a/\mathrm{d}t$ is the velocity of the CL, σ is the surface tension, α is the apparent contact angle, and α_s its equilibrium/static value. The slip coefficient λ, as well as the parameter ϵ based on it, reflect molecular processes in the vicinity of the moving CL. The apparent angle α can, however, be affected by the hydrodynamics of the overall squeezing flow in the bulk, which should be found as a solution of the problem. The way the macroscopic flow affects propagation of the CL predicted via (8), is the main question of the present work.

Incorporation of such effects as the London-van der Waals forces in the vicinity of the CL results in a law for the CL motion similar to (8), with the slip coefficient λ and the constant ϵ determined by these forces. We shall consider (8) as the boundary condition at the CL. It will be shown in Section 4 that this condition can only be used for the initial stage of the process, and it will be discussed there again for the cases when rolling motion sets in at the CL.

Using the symmetry of the solution about the axes of coordinates, we obtain the following boundary conditions:

$$u_y = 0, \quad \frac{\partial u_x}{\partial y} = 0, \quad y = 0, \tag{11}$$

$$u_x = 0, \quad \frac{\partial u_y}{\partial x} = 0, \quad x = 0. \tag{12}$$

Note that the second of conditions in (11) and (12) can be rewritten in the form

$$f_x = 0, \quad y = 0, \tag{13}$$

$$f_y = 0, \quad x = 0, \tag{14}$$

where

$$f_i = \Pi_{ik} n_k, \quad i,k = \{x,y\} \tag{15}$$

are the stress components, **n** is a unit normal vector to an appropriate surface.

The dynamic boundary conditions at the free surface are given by

$$\mathbf{f}\cdot\boldsymbol{\tau}=0, \tag{16}$$

$$\mathbf{f}\cdot\mathbf{n}=\sigma\kappa, \tag{17}$$

where $\boldsymbol{\tau}$ and **n** are the unit tangent and normal vectors at the free surface, and κ is the curvature of the free surface.

Eqs. (16) and (17) reflect the fact that the shear stress at the free surface vanishes whereas the normal stress exhibits a jump due to the Laplace pressure. The kinematic boundary condition at the free surface reads

$$\frac{\mathrm{d}\mathbf{r}}{\mathrm{d}t}=\mathbf{u}(\mathbf{r},t), \tag{18}$$

where **r** is the radius vector of a material point of the surface. The initial values of **r** are given on the circular arcs,

$$\mathbf{r}(0)=\mathbf{r}^0, \tag{19}$$

where $\mathbf{r}(0)$ is the initial position of the surface point on the circular meniscus (cf. Fig. 1).

3. Numerical method of solution

In the governing equations, time is rendered dimensionless by $\mu h_0/\sigma$, the coordinates by h_0, the velocity components by σ/μ, the pressure and stresses by σ/h_0, the half-gap between the plates by h_0, and the curvature of the free surface by $1/h_0$.

Eq. (18) can be integrated numerically using the Kutta–Merson method, provided the surface velocity is known at any given moment of time. The latter is found from the Stokes Eqs. (2) and (3) with the boundary conditions (6), (11) and (12) (or, equivalently, (13)–(15)), (16) and (17). The problem can be solved numerically using the boundary element method (BEM), successfully applied in the past to various elastostatic (Becker, 1992) and hydrodynamic problems at low Reynolds numbers (Pozrikidis, 1992, van de Vorst, 1994, Kelmanson, 1983). Its implementation in the present case is similar to those of the above. We can find the unknown velocity (stress) components on that part of the boundary where the corresponding stress (velocity) components are known. The additional condition at the moving CL was implemented using (8), which in dimensionless form reads

$$u_x(a,h)=\epsilon(G(\alpha)-G(\alpha_s)). \tag{20}$$

This condition yields the value of the slip velocity at the CL as it moves along the plates during squeezing. The apparent contact angle α is calculated as

$$\alpha=\begin{cases}\arctan\left(\dfrac{\partial\zeta}{\partial x}|_{x=a}\right), & \text{if } \dfrac{\partial\zeta}{\partial x}|_{x=a}>0,\\[2ex] \pi+\arctan\left(\dfrac{\partial\zeta}{\partial x}|_{x=a}\right), & \text{if } \dfrac{\partial\zeta}{\partial x}|_{x=a}<0,\end{cases} \tag{21}$$

where the function $\zeta(x)$ gives the surface shape. Since the surface shape is affected by the bulk flow due to squeezing, the velocity of the CL is also affected by the bulk flow via Eqs. (20) and (21).

The contribution of the singular part of the stresses is of order $\mu U/r$ (where r is the distance from the CL (Moffatt, 1964)) and concentrated in the vicinity of the CL (in a region of size ϵh_0). It cannot influence the flow far from the CL. The bulk flow forced by the squeezing determines the apparent contact angle, hence the velocity of the CL. Therefore, to solve the problem in the bulk we do not need any model dealing with the stress singularity.

High accuracy of the calculations was achieved through fine resolution of the boundary near the CL, and using a non-uniform boundary grid with small elements. With the velocity at the free surface found using BEM, Eq. (18) is integrated, yielding a step in the time evolution of the boundary.

4. Results and discussion

The results will be discussed using two dimensionless groups: the one based on the plate velocity, $\overline{V} = \mu V/\sigma$, and the transient one $\mathrm{Ca_t}(t) = \mu(\mathrm{d}a/\mathrm{d}t)/\sigma$, which is the transient capillary number based on the velocity of the CL. The time evolution of the free surface of a liquid is illustrated in Figs. 2 and 3 for $\overline{V} = 2.5$ and 5 respectively, with $l_0/h_0 = 2$. The initial apparent contact angle and stationary contact angle were taken as $\alpha_s = \pi/3$. The upper plate moves downwards from $y = 1$, and the free surface (which initially met the upper plate at $x = 2$, $y = 1$) meets it at $x > 2$ and $y < 1$.

The initial stage of the squeezing process for $\overline{V} = 0.05 - 2.5$ is shown in Figs. 4–6 in detail. From these figures, we see that at the initial stage the originally concave free surface evolves into a convex one. The apparent contact angle increases gradually and approaches π at some moment of time which represents the onset of rolling motion. The reason for this is that the wetting rate of the CL (predicted by (8) and determined by the molecular processes at a short distance from it, of the order of ϵh_0) is much lower than the squeezing rate. The flow velocity in the x-direction over the free surface is much higher than the molecular slip at the CL, which leads to a continual increase of the apparent contact angle. This enables us to conclude that under sufficiently strong squeezing, the evolution of the angle is strongly affected by the bulk flow which overbears the molecular effects and rolling motion inevitably sets in.

The transient Reynolds number can be estimated using the analytical solution in the bulk of the liquid (Eq. (24)). The ratio of the inertial to viscous terms in the Navier–Stokes equation yields $Re_t \sim \rho V h(t)/\mu$. Then as $h(t)$ decreases with time, the transient Reynolds number also decreases and the inertialess approximation is correct at $t > 0$ if it was correct at $t = 0$. The values of the transient capillary number $\mathrm{Ca_t}$ corresponding to Figs. 2–6 are shown in Fig. 7. It is seen that $\mathrm{Ca_t}$ increases with time. The sharp jump on all curves corresponds to the transition to rolling motion at the CL.

For small values of $\overline{V}$ the transient capillary number $\mathrm{Ca_t}$ in the calculations was sufficiently small, and the surface tension dominated the balance of the normal stresses. As a result, the shape of the free surface is almost circular as per Fig. 4. For larger $\overline{V}$, the circular approximation of the free surface during its evolution becomes poor (Figs. 5 and 6), since the viscous stresses become comparable to the surface tension effects.

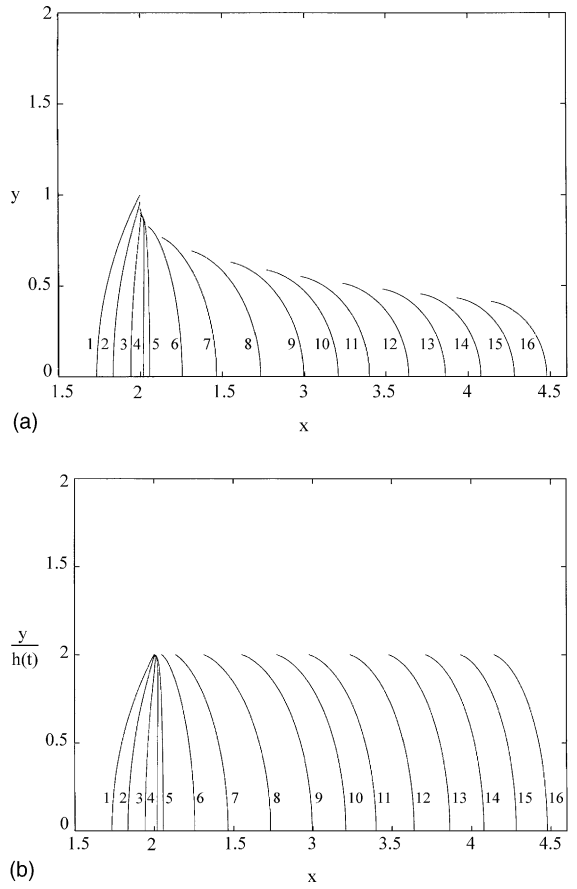

Fig. 2. Evolution of the free surface for $\overline{V} = 2.5$; $l_0/h_0 = 2$. The initial apparent contact angle $\alpha = \pi/3$. Curve 1 corresponds to $t = 0$, (2) $t = 0.015$, (3) $t = 0.03$, (4) $t = 0.04$, (5) $t = 0.045$, (6) $t = 0.069$, (7) $t = 0.094$, (8) $t = 0.12$, (9) $t = 0.15$, (10) $t = 0.17$, (11) $t = 0.18$, (12) $t = 0.195$, (13) $t = 0.207$, (14) $t = 0.217$, (15) $t = 0.226$, (16) $t = 0.234$. (a) Plotted using x, y coordinates, (b) plotted using x, $y/h(t)$ coordinates.

The numerical calculations show that the nodes at the free surface near the CL move towards the plate, to which they should reach when the apparent contact angle reached π. The velocity of the CL during the rolling motion is independent of the molecular processes and is mainly governed by the squeezing rate. Therefore, after the value of α has reached π, one can disregard the molecular wetting processes near the CL and impose as a boundary condition over the whole plate

$$u_x = 0, \quad u_y = -\overline{V}, \qquad \text{at } y = h,\ 0 \leqslant x \leqslant a. \tag{22}$$

The stress singularity at the CL is absent in this case (Dussan and Davis, 1974).

To describe numerically the evolution of the free surface at the rolling stage, node redistribution is carried out at each time step. When at some moment of time some of the nodes of the free surface near the CL stick to the plate, they should be excluded from consideration and a new CL position determined as the intersection between the surface and the plate. After that, new nodes

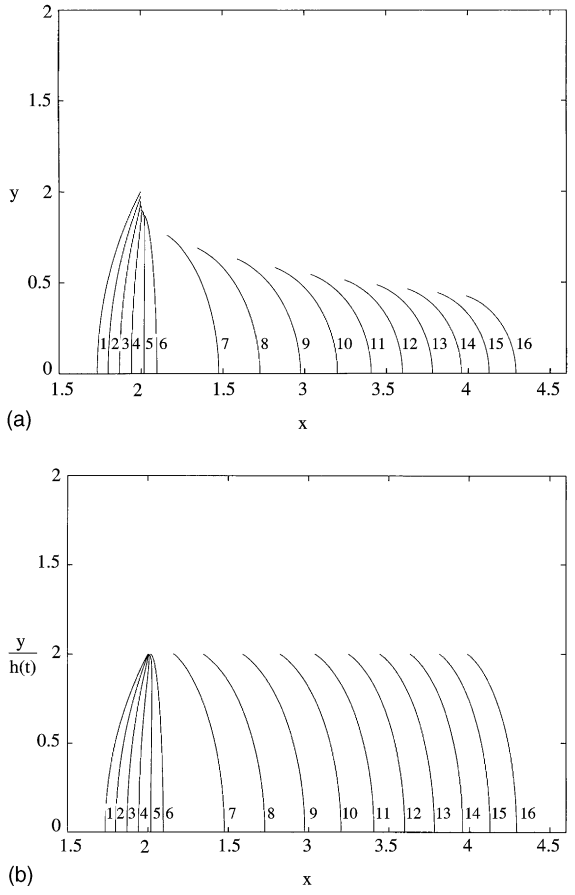

Fig. 3. Evolution of the free surface for $\overline{V} = 5$; $l_0/h_0 = 2$. The initial apparent contact angle $\alpha = \pi/3$. Curve 1 corresponds to $t = 0$, (2) $t = 0.005$, (3) $t = 0.01$, (4) $t = 0.015$, (5) $t = 0.02$, (6) $t = 0.025$, (7) $t = 0.048$, (8) $t = 0.062$, (9) $t = 0.074$, (10) $t = 0.084$, (11) $t = 0.091$, (12) $t = 0.097$, (13) $t = 0.1$, (14) $t = 0.107$, (15) $t = 0.11$, (16) $t = 0.115$. (a) Plotted using x, y coordinates, (b) plotted using x, $y/h(t)$ coordinates.

are set on the free surface with fine resolution near the new position of the CL (which is essential for accurate description of rolling), and the next time step is carried out.

At the late stage of squeezing as a/h becomes much larger than 1, the free surface does not affect the flow far from it. The flow in the bulk is accurately represented by the stream function (Laun et al., 1999)

$$\Psi_0 = \frac{3}{2} Vx\left(z - \frac{z^3}{3}\right), \quad z = \frac{y}{h}, \tag{23}$$

and

$$u_{x0} = \frac{3}{2} V \frac{x}{h}\left(1 - z^2\right), \qquad u_{y0} = -\frac{3}{2} V\left(z - \frac{1}{3} z^3\right). \tag{24}$$

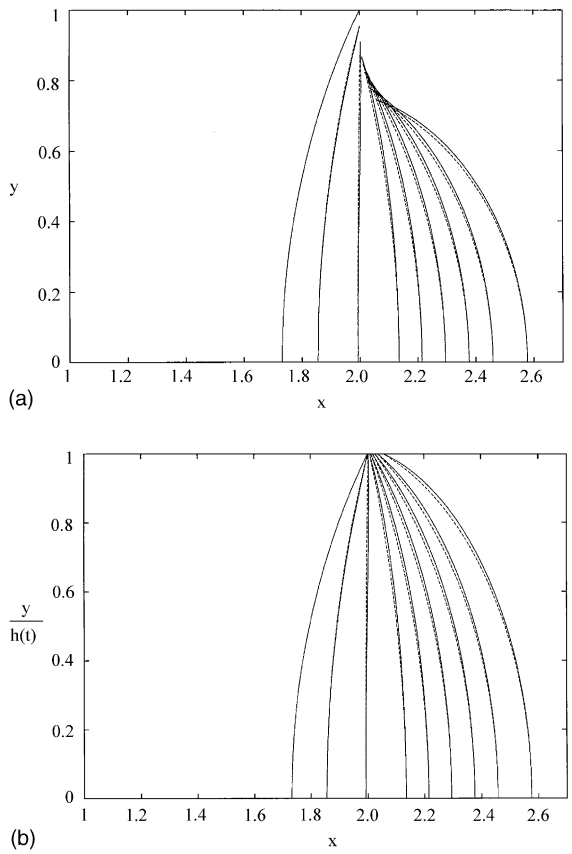

Fig. 4. Initial stage of the evolution of the free surface for $\overline{V} = 0.05$ and $l_0/h_0 = 2$. The initial apparent contact angle $\alpha = \pi/3$. Time interval between the curves $\Delta t = 0.9$ beginning from $t = 0$. Solid curves—numerical results, dashed ones (almost merging)—the corresponding approximation of the free surface by a circular arc. (a) Plotted using x, y coordinates, (b) plotted using x, $y/h(t)$ coordinates.

At the late stage the ratio u_{x0}/u_{y0} in the bulk is of the order of $a/h \gg 1$, therefore the bulk flow actually resembles Poiseuille flow in a channel.

The order of the viscous shear stresses can be estimated as $\tau_{xy} \simeq \mu(\mathrm{d}a/\mathrm{d}t)/h$, and that of the capillary pressure p_σ as $p_\sigma \simeq \sigma/h$. Their ratio is $\tau_{xy}/p_\sigma = \mu(\mathrm{d}a/\mathrm{d}t)/\sigma = \mathrm{Ca_t}$. At the late stage $\mathrm{Ca_t} \gg 1$ (cf. Fig. 7). Therefore the surface tension becomes negligibly small compared to the viscous forces, and can be disregarded when the leading term in the expansion of the solution in powers of $1/\mathrm{Ca_t}$ is sought for the late stage.

At this stage, in the leading order approximation, the bulk solution (24) can be used, say, inside the rectangle to the left of the line $(x - a)/h = -10$, to avoid an enormous increase in the number of boundary elements necessary to make calculations for a long strongly squeezed drop. However, near the free surface, at $|x| > a$, a numerical solution is constructed using BEM. At, say, $(x - a)/h = -10$ the numerical solution matches that of Eq. (24), whereas at the free surface, in the leading order, satisfies the dynamic conditions of negligible (zero) stresses. Since the flow

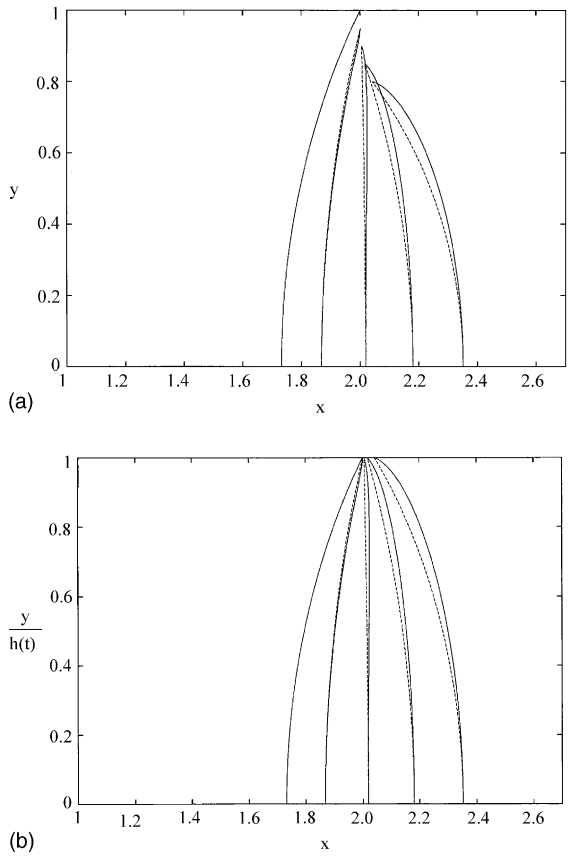

Fig. 5. Initial stage of the evolution of the free surface for $\overline{V} = 0.5$ and $l_0/h_0 = 2$. The initial apparent contact angle $\alpha = \pi/3$. Time interval between the curves $\Delta t = 0.1$ beginning from $t = 0$. Solid curves—numerical results, dashed ones—the corresponding approximation of the free surface by a circular arc. (a) Plotted using x, y coordinates, (b) plotted using x, $y/h(t)$ coordinates.

velocity and the stresses are given over the whole boundary of the region between $(x - a)/h = -10$ and the free surface, the kinematic condition

$$u_n = \frac{da/dt + \partial\zeta/\partial t}{\left[1 + (\partial\zeta/\partial y)^2\right]^{1/2}} \tag{25}$$

cannot be satisfied for all shapes of the free surface $x - a = \zeta(t, y)$, but only for a specific one; u_n is the normal velocity at the free surface. Moreover, since at the late stage $da/dt \gg \partial\zeta/\partial t$, the kinematic condition reduces to

$$\frac{u_n}{da/dt} = \frac{1}{\left[1 + (\partial\zeta/\partial y)^2\right]^{1/2}}, \tag{26}$$

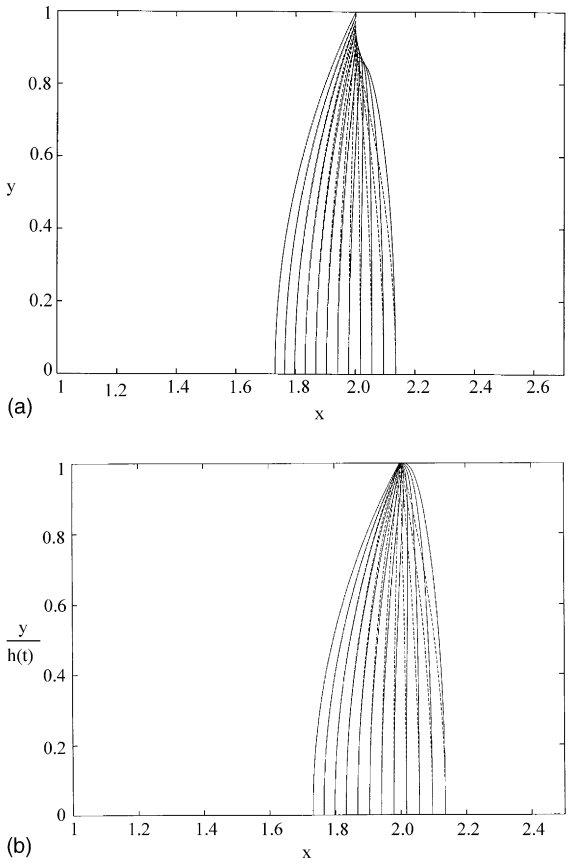

Fig. 6. Initial stage of the evolution of the free surface for $\overline{V} = 2.5$ and $l_0/h_0 = 2$. The initial apparent contact angle $\alpha = \pi/3$. Time interval between the curves $\Delta t = 0.005$ beginning from $t = 0$. Solid curves—numerical results, dashed ones—corresponding approximation of the free surface by a circular arc. (a) Plotted using x, y coordinates, (b) plotted using x, $y/h(t)$ coordinates.

Eq. (26) shows that in the leading order approximation in terms of $1/\mathrm{Ca_t}$, in the frame of reference associated with the moving CL the flow in the tip $(x-a)/h > -10$ does not depend on time (i.e. ζ/h depends only on $z = y/h$).

BEM was employed to calculate the flow, as well as to find the fully developed shape of the free surface via iterations based on Eq. (26). The results for the leading order in $1/\mathrm{Ca_t}$ are shown in Fig. 8. It is seen that the shape of the free surface (curve 1) achieved at the late stage differs from a circle (curve 2). It is emphasized that the calculated fully developed shape (curve 1 in Fig. 8) corresponds to rolling motion with the apparent contact angle $\alpha = \pi$.

Denote $\overline{x}_1 = (x-a)/h$ and $\overline{y}_1 = 1 - y/h$. The local shape of the free surface 1 in Fig. 8 as $\overline{x}_1 \to 0$ and $\overline{y}_1 \to 0$ is approximated by the scaling $\overline{y}_1 = 0.28 \cdot \overline{x}_1^{1.528}$. This result is obtained for $\mathrm{Ca_t} \gg 1$. Benney and Timson (1980) calculated the local shape of the free surface near the moving CL for the case of rolling motion. In the present notation their result is $\overline{y}_1 = \mathrm{const} \cdot \overline{x}_1^q$ (cf. their Eq. (3.20)). Ngan and Dussan (1984) pointed out that the calculation of the exponent q in Benney and Timson (1980) should be corrected. The corrected equation for q given in Ngan and Dussan

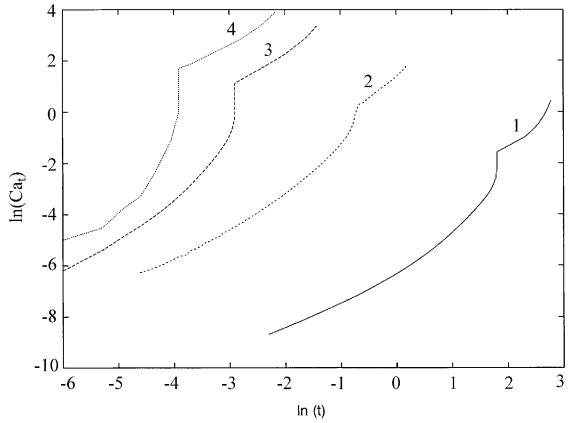

Fig. 7. Transient capillary number versus time. Curve 1 corresponds to $\overline{V} = 0.05$ (Fig. 4), (2) $\overline{V} = 0.5$ (Fig. 5), (3) $\overline{V} = 2.5$ (Figs. 2 and 6), (4) $\overline{V} = 5.0$ (Fig. 3).

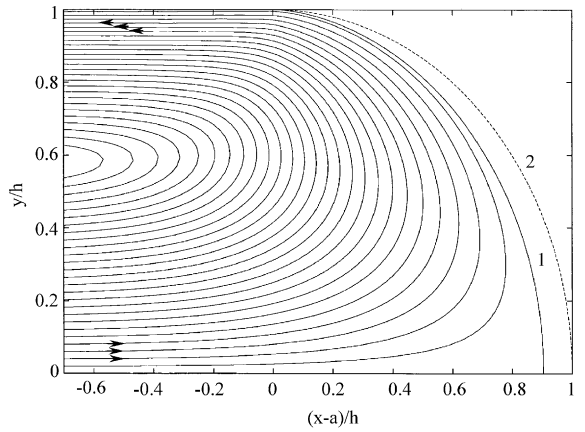

Fig. 8. Flow in the tip near the free surface at the remote stage of squeezing. Curve 1 shows the calculated shape of the free surface with the apparent contact angle $\alpha = \pi$, which corresponds to rolling motion. The shape is "saturated" in the leading order approximation in terms of $1/\mathrm{Ca_t}$. It is rather close to a circle (curve 2), albeit different from it. All the other curves show the streamlines of the flow in the frame of reference associated with the moving CL.

(1984) in the present notation has the form $\tan(q\pi) = -2\mathrm{Ca_t}$. The solution of this equation for $\mathrm{Ca_t} \gg 1$ eliminating infinite forces at the CL is given by q tending to $3/2$ from above. Therefore the prediction of these two works is in agreement with the result of the present one. It is interesting to note that the free surface cusps at large capillary numbers follow the same asymptotics $\overline{y}_1 = \mathrm{const} \cdot \overline{x}_1^{3/2}$ (Joseph et al., 1991; Jeong and Moffatt, 1992).

The area of the drop cross-section S is given by

$$S = 2ah + C \cdot h^2, \tag{27}$$

where

$$C = \int_0^1 \overline{\zeta}(z)\,\mathrm{d}z, \quad \overline{\zeta} = \frac{\zeta}{h}. \tag{28}$$

For the late stage the value of the constant C is readily found using the calculated free surface shape ζ.

Differentiating (27) in time, and using the constant volume condition, we find

$$\frac{\mathrm{d}a}{\mathrm{d}t} = -\left(\frac{a}{h} + C\right)\frac{\mathrm{d}h}{\mathrm{d}t}. \tag{29}$$

For the late stage $a/h \gg C$, and Eq. (29) reduces to

$$\frac{\mathrm{d}a}{\mathrm{d}t} = -\frac{a}{h}\frac{\mathrm{d}h}{\mathrm{d}t}, \tag{30}$$

which yields

$$a = \frac{K}{h}, \tag{31}$$

where K is a constant.

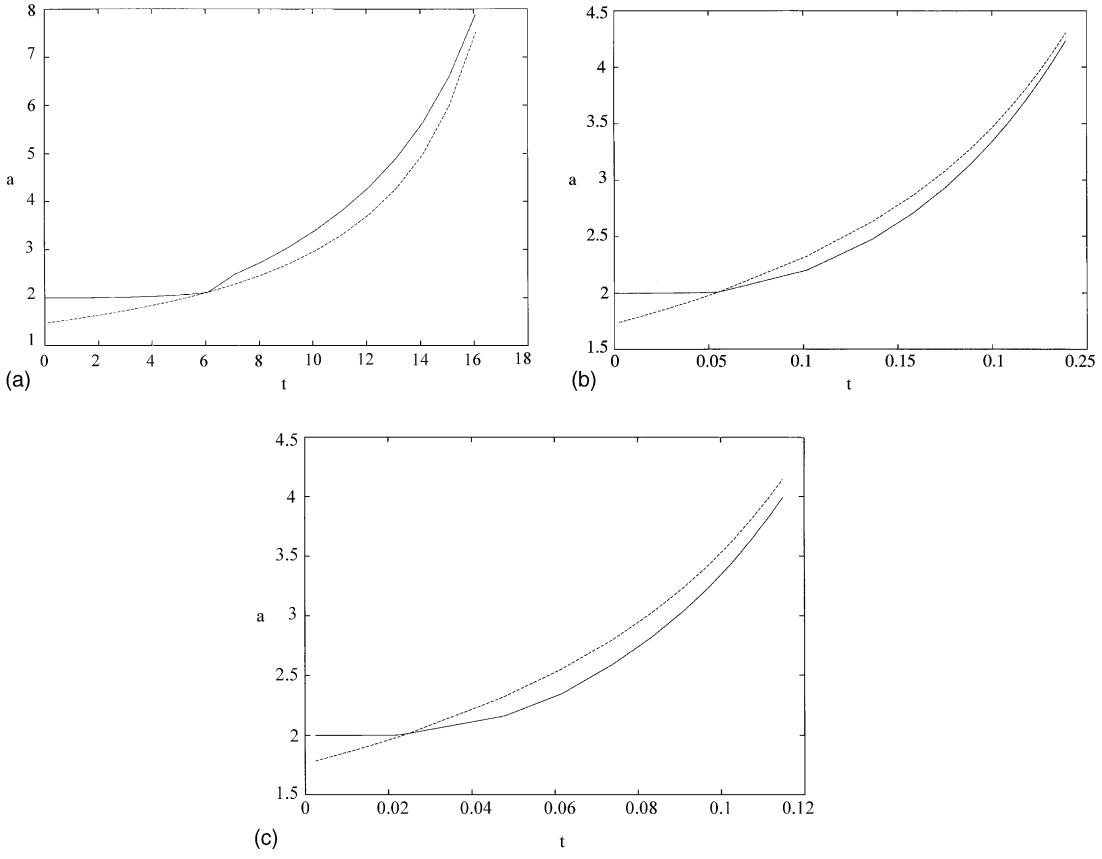

Fig. 9. Dependence of the coordinate of the CL $x = a(t)$ on time. (a) $\overline{V} = 0.05$, (b) $\overline{V} = 2.5$, (c) $\overline{V} = 5$. Solid lines—numerical results, the dashed ones—the analytical ones, Eq. (32).

In the dimensionless form $h = 1 - \overline{V}t$. If the late stage begins at $t = t_* < 1/\overline{V}$ (when $a = a_*$), which is characterized, say, by the onset of rolling motion, Eq. (31) yields

$$a = a_* \frac{1 - \overline{V}t_*}{1 - \overline{V}t}. \tag{32}$$

The numerically obtained dependence of the x coordinate of the CL a on time is compared to the asymptotic one from (32) in Fig. 9. The two results draw closer as t increases.

5. Conclusion

Squeezing of a two-dimensional droplet between parallel plates moving with a constant velocity against one another represents a convenient model for the analysis of the dynamics of moving CLs. The flow is also of significant interest in a number of applications. The initial shape of the free surface was assumed to be circular. However, at the beginning of the squeezing process, there is a period when the free surface deviates from circularity, while the apparent contact angle is less than π. This effect is stronger for higher values of the dimensionless velocity $\overline{V}$. This period is longer for lower values of $\overline{V}$ (lower squeezing rate). Under sufficiently strong squeezing, the overall dynamics of the CL is mainly governed by the macroscopic (squeezing) bulk flow, whereas the molecular processes leading to slip and wetting in the vicinity of the CL have a minor effect. As a result, the apparent contact angle gradually increases and reaches the value of π at some moment of time depending on the value of $\overline{V}$. Then rolling motion of the CL sets in. At this stage, as time increases, the gap between the plates becomes small relative to the length of the droplet and the free surface tends to a steady-state fully developed shape close to a circle, albeit different from it.

Acknowledgements

This research was partially supported by GIF—the German–Israeli Foundation for Scientific Research and Development, research grant no I-536-097.14/97. S.N. Reznik acknowledges support by the Center for Absorption in Science, Ministry of Immigrant Absorption (State of Israel).

References

Babsky, V.G., Kopachevsky, N.D., Myshkis, A.D., Slobozhanin, L.A., Tyuptsov, A.D., 1987. Low-Gravity Fluid Mechanics. Mathematical Theory of Capillary Phenomena. Springer, Berlin.

Becker, A.A., 1992. The Boundary Element Method in Engineering. A Complete Course. McGraw-Hill, New York.

Benney, D.J., Timson, W.J., 1980. The rolling motion of a viscous fluid on and off a rigid surface. Stud. Appl. Math. 63, 93–98.

Bezdenejnykh, N.A., Meseguer, J., Perales, J.M., 1999. An experimental analysis of the instability of nonaxisymmetric liquid bridges in a gravitational field. Phys. Fluids 11, 3181–3185.

Blake, T.D., 1993. Dynamic contact angles and wetting kinetics. In: Berg, J.C. (Ed.), Wettability. Marcel Dekker, New York, pp. 251–309.

Cox, R.G., 1986. The dynamics of the spreading of liquids on a solid surface. Part 1. Viscous flow. J. Fluid Mech. 168, 169–194.

Dussan V, E.B., 1979. On the spreading of liquids on solid surfaces: static and dynamic contact lines. Ann. Rev. Fluid Mech. 11, 371–400.

Dussan V, E.B., Davis, S.H., 1974. On the motion of a fluid-fluid interface along a solid surface. J. Fluid Mech. 65, 71–95.

Harsh, K.F., Bright, V.M., Lee, Y.C., 1999. Solder self-assembly for three-dimensional microelectromechanical systems. Sens. Actuators, A (Physical) 77, 237–244.

Hayes, R.A., Ralston, J., 1993. Forced liquid movement on low energy surfaces. J. Colloid Interface Sci. 153, 429–438.

Hoffman, R., 1975. A study of the advancing interface. I. Interface shape in liquid–gas systems. J. Colloid Interface Sci. 50, 228–241.

Jeong, J.-T., Moffatt, H.K., 1992. Free surface cusps associated with flow at low Reynolds number. J. Fluid Mech. 241, 1–22.

Joseph, D.D., Nelson, J., Renardy, M., Renardy, Y., 1991. Two-dimensional cusped interfaces. J. Fluid Mech. 223, 383–409.

Kelmanson, M.K., 1983. An integral equation method for the solution of singular slow flow problems. J. Comput. Phys. 51, 139–158.

Laun, H.M., Rady, M., Hassager, O., 1999. Analytical solutions for squeeze flow with partial wall slip. J. Non-Newtonian Fluid Mech. 81, 1–15.

Moffatt, H.K., 1964. Viscous and resistive eddies near a sharp corner. J. Fluid Mech. 18, 1–18.

Ngan, C.G., Dussan V, E.B., 1984. The moving contact line with a180° advancing contact angle. Phys. Fluids 27, 2785–2787.

Patra, S.K., Sritharan, S.S., Lee, Y.C., 1995. Quantitative characterization of a flip–chip solder joint. Trans. ASME, J. Appl. Mech. 62, 390–397.

Pozrikidis, C., 1992. Boundary Integral and Singularity Methods for Linearized Viscous Flow. Cambridge University Press, Cambridge.

Rioboo, R., Tropea, C., Marengo, M., 2001. Outcomes from a drop impact on solid surface. Atomization Sprays 11, 155–165.

Somalinga, S., Bose, A., 2000. Numerical investigation of boundary conditions for moving contact line problems. Phys. Fluids 12, 499–510.

van de Vorst, G.A.L., 1994. Ph.D. Thesis. Modeling and numerical simulation of viscous sintering. Febodruk-Enschede, The Netherlands.

Weiss, D.A., Yarin, A.L., 1999. Single drop impact onto liquid films: neck distortion, jetting, tiny bubble entrainment, and crown formation. J. Fluid Mech. 385, 229–254.

Yarin, A.L., Weiss, D.A., 1995. Impact of drops on solid surfaces: self-similar capillary waves, and splashing as a new type of kinematic discontinuity. J. Fluid Mech. 283, 141–173.

Zayas, F., Alexander, J.I.D., Meseguer, J., Ramus, J.F., 2000. On the stability limits of long non-axisymmetric cylindrical liquid bridges. Phys. Fluids 12, 979–985.